International Journal of Heat and Mass Transfer 164 (2021) 120538

Contents lists available at ScienceDirect

International Journal of Heat and Mass Transfer

journal homepage: www.elsevier.com/locate/hmt

Local thermal non-equilibrium (LTNE) model for developed flow in porous media with spatially-varying Biot number

Mohammad Parhizi, Mohsen Torabi, Ankur Jain*

Mechanical and Aerospace Engineering Department, University of Texas at Arlington, Arlington, TX, USA

ARTICLE INFO

Article history:
Received 24 June 2020
Revised 23 September 2020
Accepted 26 September 2020

Keywords:
Porous medium
Heat transfer
Local thermal non-equilibrium
Fully developed internal flow
Variable Biot number

ABSTRACT

The local thermal non-equilibrium (LTNE) model has been extensively used to model convective heat transfer in porous media. Most of the past LTNE-based models account for thermal interactions between fluid and solid phases in the form of a constant Biot number (*Bi*). This work presents a local thermal non-equilibrium model for fully developed flow in a channel filled with a porous medium where *Bi* itself varies across the channel. A set of differential equations for fluid and solid phase temperature fields are derived under this condition, which are shown to be generalizations of previously presented results for constant *Bi*. Results from the present analysis are shown to reduce to and agree with past work for the special case of constant *Bi*. The variable *Bi* model is used to investigate the effect of thermal properties such as thermal conductivity on the fluid and solid temperature profiles. The nature of temperature distributions are correlated with the spatial variation in *Bi*, including for parabolic and sinusoidal variation. Specifically, for periodic *Bi*, the locations of maxima and minima in temperature fields are found to be well correlated with corresponding maxima and minima in *Bi*. Nusselt number (*Nu*) for different values of thermal conductivities and heat generation rates are determined for variable *Bi*. This work accounts for an important physical consideration in porous media and generalizes previously-presented LTNE models for porous media in a channel.

1. Introduction

Fluid flow and heat transfer in a porous medium is a problem of much theoretical and practical importance [1–4]. Thermal and fluid transport in porous media occur in a wide variety of engineering applications, including electronics cooling [5], oil and gas extraction [6], bioengineering [7] and energy storage [8]. A typical scenario in a porous medium involves fluid flow through a two-phase region comprising solid and fluid phases with a certain porosity, along with heat exchange with the surroundings through appropriate boundary conditions. A wide variety of coupled and often non-linear physical processes have been modeled and analyzed in the context of heat transfer and fluid flow in a porous medium. The comprehensive literature in this field has been summarized in well-known handbooks [1–4].

The simplest approach for solving porous medium heat transfer problems involves the assumption of local thermal equilibrium (LTE) between the solid and liquid phases of the porous medium [9]. The LTE assumption may be valid when the solid and fluid phases do not locally exchange heat, or when the thermal conductivities of the two phases are similar, leading to equal local temperature of the two phases. In contrast, an alternate approach of local thermal non-equilibrium (LTNE) has been developed in the past few decades [10,11] to account for local heat exchange and local temperature difference between the two phases. In the LTNE approach, the solid and fluid temperature fields are assumed to be distinct, and coupled with each other through a local convective heat transfer coefficient that governs the rate of local heat exchange between the two phases. The LTNE approach has been used for modeling heat transfer in porous media in a variety of scenarios. For example, LTNE condition has been used to investigate temperature gradient bifurcation in a channel filled with a porous medium [11]. Analytical solutions and their limitations for different conditions at the porous-fluid interface have been discussed heat transfer due to natural convection in a porous media using both LTE and LTNE conditions has been investigated [12]. Different types of boundary conditions for transpiration cooling have been investigated using a LTNE model [13]. Exact solutions for heat transfer and fluid flow in a partially porous parallel-plate [14] and a pipe [15] with LTNE conditions have been presented. Results showed that the Nusselt number is greater in partially porous channels compared to a fully porous channel. Temperature distribution and Nusselt number in a partially filled channel for two different in-

* Corresponding author.
E-mail address: jaina@uta.edu (A. Jain).

https://doi.org/10.1016/j.ijheatmasstransfer.2020.120538
0017-9310/

Nomenclature

Bi	Biot number, $Bi(\eta) = \frac{h_i \alpha H^2}{k_{s,eff}}$
c_p	specific heat of the fluid (J kg^{-1} K^{-1})
h_i	interstitial heat transfer coefficient (W m^{-2} K^{-1})
h_w	wall heat transfer coefficient (W m^{-2} K^{-1})
H	half height of the channel (m)
K	permeability (m^{-2})
k	ratio of thermal conductivities, $k = \frac{k_{f,eff}}{k_{s,eff}}$
k_{eff}	effective thermal conductivity (W m^{-1} K^{-1})
Nu	Nusselt number
p	pressure (N m^{-2})
q_w	heat flux at the wall (W m^{-2})
S	internal heat generation (W m^{-3})
T	temperature (K)
u	fluid velocity (m s^{-1})
x	horizontal coordinate (m)
y	vertical coordinate (m)
α	specific interfacial area in the porous medium (m^{-1})
β	non-dimensional heat generation parameter, $\beta = \frac{S_s H}{q_w}$
η	non-dimensional coordinate, $\eta = \frac{y}{H}$
μ	dynamic viscosity (kg m^{-1} s^{-1})
θ	non-dimensional temperature, defined as $\theta = \frac{k_{s,eff}(T-T_w)}{Hq_w}$ for model A and $\theta = \frac{k_{s,eff}(T-T_{s,w})}{Hq_w}$ for model B
$\theta_{f,b}$	non-dimensional bulk mean temperature of the fluid
ω	non-dimensional frequency

Subscripts

f	fluid
s	solid
w	wall

terface heat flux conditions – equal heat flux between the two phases and heat flux division based on the thermal conductivities of the two phases – were investigated and compared [16,17]. Thermal behavior and entropy generation rate in a channel with a partially porous medium under LTNE conditions has been investigated [18]. Heat transfer in the thermally developing region [19,20] and in the slip regime [21] has been modeled. Exact solutions for conjugate heat transfer involving porous media have been presented [22]. An exact solution has also been presented for pulsating flow in a porous medium under the LTNE assumption [23].

The modeling of two different temperature fields for the solid and fluid phases in the LTNE approach necessitates careful consideration of the boundary condition on the domain surfaces. For example, in flow through a channel filled with a porous medium and heated up from the channel wall, the thermal boundary condition is quite straightforward for the LTE approach. However, in the LTNE approach, the distribution of the wall heat flux between the solid and fluid phases is not clear. To address this problem, two distinct models have been proposed [24,25]. In a model commonly referred to as model A, the temperature of the solid and fluid phases at the wall are assumed to be the same as the wall temperature [24]. Model B, on the other hand, assumes the heat flux into the solid and fluid phases to both be equal to the imposed wall heat flux [25]. Both models result in distinct temperature distributions and temperature bifurcation between the two phases, which has been studied in detail, including the effect of internal heat generation and thermal properties [11,26]. The LTNE approach has also been analyzed in the context of a channel that is filled partially with a porous medium, and the rest with a pure fluid [26], as such scenarios are of practical importance in microreactors and other applications [27].

A key feature of the LTNE approach is the local interstitial heat transfer coefficient, h, that governs local heat transfer between the two phases. This term appears in the local convective heat transfer term in the governing energy equation for the solid and fluid temperatures, typically removing heat from one equation and adding it to the other [10,24]. When non-dimensionalizing the equations, this term leads to the Biot number, Bi, given by $Bi = \frac{h_i \alpha H^2}{k_{s,eff}}$, where α is the interfacial area per unit volume, $k_{s,eff}$ is the effective thermal conductivity of the solid phase and H is the channel half-width. Most of the LTNE literature assumes Bi to be a constant parameter [10,11,24,25], and analyzes the impact of the value of Bi on temperature distribution, temperature bifurcation between the phases, and the wall heat transfer. However, there may be practical scenarios where Bi may not be constant throughout the channel due to spatial variations in one or more parameters that constitute Bi. For example, α may vary over the channel if the porous medium does not have uniform composition. For example, it is possible to design functionally graded materials with spatially varying interfacial area per unit volume [28]. Spatial variations in Bi may also occur due to manufacturing variations or defects. The local convective heat transfer coefficient may also vary over the channel due to flow variations. In scenarios where such effects may be important, the traditional LTNE approach of assuming constant Bi may need to be generalized. Some past work is available on analysis of heat transfer in layered porous media, where each layer may have a distinct Bi [29,30]. However, it is desirable to generalize this to a situation where Bi varies smoothly over the entire porous medium. Specifically, periodic or polynomial spatial distribution of Bi may be of particular interest, since distributions of other nature can be modeled on the basis of such simpler, fundamental functions.

This paper presents theoretical analysis of temperature distribution in a channel filled with a porous medium using the LTNE approach while assuming a non-uniform distribution of the Biot number. Fourth-order ordinary differential equations (ODEs) for the solid and fluid temperatures are derived. These ODEs are generalizations of prior results that were based on the assumption of constant Bi. While analytical solutions for these ODEs are difficult to obtain for even the simplest Bi distribution, the equations can be easily solved numerically. Solutions of the governing ODEs are analyzed to understand the effect of Biot number distribution on the temperatures of the two phases, the thermal bifurcation and heat exchange with the wall as represented by the Nusselt number. The theoretical results discussed in this paper generalize the constant Bi LTNE approach for a practically relevant scenario, and may be of importance in multiple engineering applications.

2. Mathematical modeling

Fig. 1 shows a schematic of the geometry under consideration. A channel of half-width H and fully filled with a porous medium subjected to steady, incompressible and laminar fluid flow across the channel and uniform heat flux from the channel wall. Thermally and hydrodynamically developed conditions are assumed. A variation in the Biot number is assumed in the y direction, described by a given functional form. A uniform fluid flow is assumed, which is governed by Darcy model due to the small value of the microscale Reynolds number [31]. Internal heat generation is assumed to occur in the fluid and solid phases, which could be due to chemical reaction, conversion of electrical energy into heat or radiative absorption [27]. All parameters are assumed to be temperature-independent. Thermal dispersion effects [32] are neglected. Heat transfer due to radiation and natural convection is

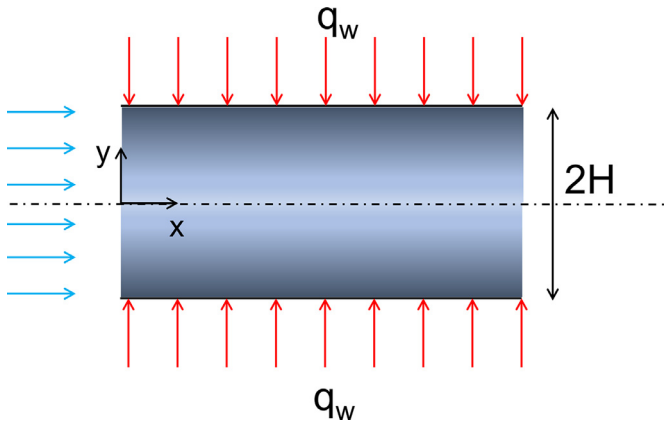

Fig. 1. Schematic of the problem comprising a porous channel with spatially-varying Biot number. The channel is being heated with constant heat flux from the wall.

assumed to be negligible. Viscous heat dissipation is also ignored. Under these assumptions, the momentum equation for fluid flow is given by the Darcy model:

$$-\frac{\mu_f}{K}u = \frac{dp}{dx} \tag{1}$$

which simply indicates a constant fluid velocity in the porous medium.

The solid and fluid temperatures have been shown to be governed by the following energy conservation differential equations [11]:

$$k_{f,eff}\frac{\partial^2 T_f}{\partial y^2} + h_i\alpha\left(T_s - T_f\right) + S_f = \rho C_p u\frac{\partial T_f}{\partial x} \tag{2}$$

$$k_{s,eff}\frac{\partial^2 T_s}{\partial y^2} - h_i\alpha\left(T_s - T_f\right) + S_s = 0 \tag{3}$$

Symmetry about the center-line results in the following boundary conditions

$$\left(\frac{\partial T_f}{\partial y}\right)_{y=0} = \left(\frac{\partial T_s}{\partial y}\right)_{y=0} = 0 \tag{4}$$

Additional boundary conditions are obtained based on the assumed nature of thermal interaction between the two phases and the wall. The solution for temperature distribution with variable *Bi* is derived in the next sub-sections for two most commonly used models for this purpose.

2.1. Model A

Model A assumes the two phases to have the same temperature at the wall, i.e.

$$T_f = T_s = T_w \text{ at } y = H \tag{5}$$

To simplify, the two energy conservation equations are added and integrated over the channel to derive an expression for the advection term in Eq. (2) assuming that the total wall heat flux is equal to the addition of heat fluxes of solid and liquid phase at the wall. Doing so has been shown to result in elimination of S_f, the internal heat generation in the fluid [11]. Based on the non-dimensionalization scheme summarized in the nomenclature section, the following non-dimensional governing equations and boundary conditions can be derived for the fluid and solid phase temperature fields, θ_f and θ_s:

$$k\theta_f'' + Bi(\eta)\left(\theta_s - \theta_f\right) = 1 + \beta \tag{6}$$

$$\theta_s'' - Bi(\eta)\left(\theta_s - \theta_f\right) + \beta = 0 \tag{7}$$

$$\theta_f(1) = 0 \tag{8}$$

$$\theta_s(1) = 0 \tag{9}$$

$$\theta_f'(0) = 0 \tag{10}$$

$$\theta_s'(0) = 0 \tag{11}$$

where the prime signs refer to differentiation with respect to the spatial variable η.

The solid temperature θ_s can be written explicitly as a function of θ_f and its derivatives using Eq. (6). Similarly, Eq. (7) can be rewritten to express θ_f as a function of θ_s and its derivatives. Therefore, the following expressions can be obtained for θ_f and θ_s:

$$\theta_f = -\frac{1}{Bi}\left(\theta_s'' + \beta\right) + \theta_s \tag{12}$$

$$\theta_s = \frac{1}{Bi}\left(1 + \beta - k\theta_f''\right) + \theta_f \tag{13}$$

While past work has proceeded to uncouple and solve these equations under the assumption of a constant *Bi*, this work considers a generalized scenario where the *Bi* number varies over space, i.e. *Bi=Bi(η)*. In such a case, differentiating Eq. (12) with respect to η once and twice results in:

$$\theta_f' = -\frac{\theta_s'''}{Bi} + \frac{Bi'\theta_s''}{Bi^2} + \theta_s' + \beta\frac{Bi'}{Bi^2} \tag{14}$$

$$\theta_f'' = -\frac{\theta_s''''}{Bi} + 2\frac{Bi'}{Bi^2}\theta_s''' + \theta_s''\left(1 + \frac{Bi''}{Bi^2} - 2\frac{Bi'^2}{Bi^3}\right) + \beta\left(\frac{Bi''}{Bi^2} - 2\frac{Bi'^2}{Bi^3}\right) \tag{15}$$

where the prime signs refer to differentiation with respect to the spatial variable η.

Substituting Eq. (15) into Eq. (6) results in the following fourth order ODE for θ_s:

$$k\theta_s'''' - 2k\frac{Bi'}{Bi}\theta_s''' - Bi(1+k)\theta_s'' - k\left(\frac{Bi''}{Bi} - 2\frac{Bi'^2}{Bi^2}\right)\theta_s'' - k\beta\left(\frac{Bi''}{Bi} - 2\frac{Bi'^2}{Bi^2}\right) = -Bi \tag{16}$$

Two boundary conditions for Eq. (16) are already available in Eq. (9) and Eq. (11). Since Eq. (16) is a fourth-order differential equation, two more boundary conditions are required for the problem to be completely defined. These extra equations can be derived by using Eqs. (8)–(11) in Eq. (7). Eqs. (8) and (9) can be simply substituted in Eq. (7) and the following boundary condition for θ_s'' is obtained.

$$\theta_s''(1) = -\beta \tag{17}$$

Moreover, Eq. (7) can be differentiated, followed by use of Eqs. (10) and (11) to obtain the following boundary condition for θ_s'''.

$$\theta_s'''(0) - Bi'(0)\left(\theta_s(0) - \theta_f(0)\right) = 0 \tag{18}$$

Note that the solid and fluid temperature boundary conditions are still coupled in Eq. (18). However, since the channel is assumed to be symmetric about the center-line, it is reasonable to assume the *Bi* distribution to be symmetric as well. Therefore, $Bi'(\eta)$ must

be zero at η=0, and Eq. (18) can be simplified as follows:

$$\theta_s'''(0) = 0 \tag{19}$$

Eqs. (16), (9), (11), (17) and (19) represent the fourth-order ODE and four associated boundary conditions for the solid phase temperature distribution. Note that the ODE in Eq. (16) represents a generalization of the previously reported ODE for constant *Bi* case. Eq. (16) can be shown to reduce to the constant *Bi* case when spatial variation in *Bi* is neglected by setting all derivatives of *Bi* to zero in Eq. (16).

Unfortunately, Eq. (16) is much more complicated than the previously-reported ODE for the constant *Bi* case [11]. In the more general case considered here, an analytical solution of Eq. (16) does not appear to be possible, even for relatively simple *Bi* functions.

Similar to θ_s, the uncoupled ODE for θ_f can be derived, starting by differentiating Eq. (13) once and twice to result in

$$\theta_s' = -\frac{1+\beta}{Bi^2}Bi' + \theta_f' - k\left(\frac{\theta_f'''}{Bi} - \frac{Bi'\theta_f''}{Bi^2}\right) \tag{20}$$

and

$$\theta_s'' = -\frac{k}{Bi}\theta_f'''' + 2k\frac{Bi'}{Bi^2}\theta_f''' + \left(1 + k\frac{Bi''}{Bi^2} - 2k\frac{Bi'^2}{Bi^3}\right)\theta_f'' + (1+\beta)\left(2\frac{Bi'^2}{Bi^3} - \frac{Bi''}{Bi^2}\right) \tag{21}$$

Substituting Eq. (21) into Eq. (7) gives the fourth-order differential equation for θ_f

$$k\theta_f'''' - 2k\frac{Bi'}{Bi}\theta_f''' - Bi(1+k)\theta_f'' - k\left(\frac{Bi''}{Bi} - 2\frac{Bi'^2}{Bi^2}\right)\theta_f'' - (1+\beta)\left(2\frac{Bi'^2}{Bi^3} - \frac{Bi''}{Bi^2}\right) = -Bi \tag{22}$$

Similar to the previous case, two boundary conditions are already available from Eq. (8) and Eq. (10). Two additional boundary conditions needed to solve Eq. (22) can be obtained by utilizing Eqs. (8)–(10) as follows:

$$\theta_f''(1) = \frac{1+\beta}{k} \tag{23}$$

$$\theta_f'''(0) = 0 \tag{24}$$

Note that, similar to θ_s, the assumption of symmetric $Bi(\eta)$ about the centerline is necessary for obtaining fully uncoupled equations for θ_f. This assumption is justified because of the assumption of symmetry in the temperature fields in this problem. Similar to Eq. (16), Eq. (22) is a generalization of the constant *Bi* case presented in the past, and can be easily shown to reduce to the previously-presented result when all derivatives of *Bi* are taken to be zero.

2.2. Model B

In Model B, the heat flux into both liquid and solid phases is taken to be the wall flux q_w, i.e.,

$$q_w = k_{s,eff}\left(\frac{\partial T_f}{\partial y}\right)_{y=H} \tag{25}$$

$$q_w = k_{f,eff}\left(\frac{\partial T_f}{\partial y}\right)_{y=H} \tag{26}$$

The fluid and solid temperatures at the wall are no longer equal to each other. In this case, a commonly used non-dimensionalization scheme is [11]:

$$\theta_s = \frac{k_{s,eff}(T_s - T_{s,w})}{Hq_w} \tag{27}$$

$$\theta_f = \frac{k_{s,eff}\left(T_f - T_{s,w}\right)}{Hq_w} \tag{28}$$

where $T_{s,w}$ is the temperature of the solid at the wall. Based on these definitions, the non-dimensional governing equations and boundary conditions can be written as:

$$k\theta_f'' + Bi(\eta)\left(\theta_s - \theta_f\right) = 2 + \beta \tag{29}$$

$$\theta_s'' - Bi\left(\theta_s - \theta_f\right) + \beta = 0 \tag{30}$$

$$\theta_s(1) = 0 \tag{31}$$

$$\theta_f'(1) = \frac{1}{k} \tag{32}$$

$$\theta_s'(0) = 0 \tag{33}$$

$$\theta_f'(0) = 0 \tag{34}$$

note that Eq. (31) results from the non-dimensionalization given by Eq. (27). Similar to the process followed for model A, explicit uncoupled equations for θ_f and θ_s can be derived for model B as follows:

$$k\theta_s'''' - 2k\frac{Bi'}{Bi}\theta_s''' - Bi(1+k)\theta_s'' - k\left(\frac{Bi''}{Bi} - 2\frac{Bi'^2}{Bi^2}\right)\theta_s'' - k\beta\left(\frac{Bi''}{Bi} - 2\frac{Bi'^2}{Bi^2}\right) = -2Bi \tag{35}$$

$$k\theta_f'''' - 2k\frac{Bi'}{Bi}\theta_f''' - Bi(1+k)\theta_f'' - k\left(\frac{Bi''}{Bi} - 2\frac{Bi'^2}{Bi^2}\right)\theta_f'' - (2+\beta)\left(2\frac{Bi'^2}{Bi^3} - \frac{Bi''}{Bi^2}\right) = -2Bi \tag{36}$$

In order to derive additional boundary conditions for Eqs. (35) and (36), Eqs. (33) and (34) is substituted into Eqs. (29) and (30). Further, Eqs. (31) and (32) are substituted into Eqs. (29) and (30), respectively. Using the assumption of symmetric *Bi* about the center-line, this results in

$$\theta_s'''(0) = 0 \tag{37}$$

$$\theta_f'''(0) = 0 \tag{38}$$

$$k\theta_f''(1) - Bi(1)\theta_f(1) = 2 + \beta \tag{39}$$

$$\theta_s'''(1) + Bi'(1)\theta_f(1) - Bi(1)\left(\theta_s'(1) - \frac{1}{k}\right) = 0 \tag{40}$$

The ODE in Eq. (36), along with boundary conditions given by Eqs. (32), (34), (38) and (39) represents a well-defined set of equations for θ_f . Once the fluid temperature field is solved, the solid temperature field is also well-defined by Eqs. (31), (33), (35), (37) and (40), treating the $\theta_f(1)$ term in Eq. (40) as a given constant based on the solution of the fluid temperature distribution. Similar to model A, the differential equations for θ_f and θ_s are unlikely to have an explicit solution even for simple *Bi* expressions, and may need to be solved numerically for most practical cases.

2.3. Nusselt number calculations

Once the temperature profile is determined, the temperature of the fluid, θ_f, can be used to calculate the Nusselt number. The mathematical expression for calculating the Nusselt number for Model A is given in Yang and Vafai [11] as follows:

$$Nu = -\frac{4}{k\theta_{f,b}} \tag{41}$$

where θ_f is the non-dimensional bulk temperature defined as:

$$\theta_{f,b} = \frac{\int_{\eta=0}^{1} \theta_f(\eta) u d\eta}{\langle u \rangle} \tag{42}$$

where $\langle u \rangle$ is the average velocity over the cross section of the channel. Note that since the ODEs in this work are not solved analytically, therefore, the expression for θ_f is not available in a closed form. However, once θ_f is determined by numerically solving Eq. (22), the integration in Eq. (42) can be carried out in order to determine the Nusselt number as a function of η.

3. Results and discussion

The governing ordinary differential Eqs. (16), (22), (35) and (36) for models A and B are solved numerically using a fourth order method boundary value problem solver. In this method, the fourth-order differential equations are re-written as a system of coupled, first order ordinary differential equations of the form $y' = f(x,y)$. The solver then integrates this system of equations subject to the defined boundary conditions using a six-stage, fifth-order Runge Kutta method.

3.1. Model validation

Results from the model presented in Section 2 are first compared with past work that the present model generalizes. Yang & Vafai have presented the temperature bifurcation for a porous medium in a channel for the case of a constant *Bi* [11]. For this comparison, a constant *Bi* input is provided to the numerical code that solves the general governing equations derived in Section 2. Fig. 2 plots temperature profile in both liquid and solid regions as a function of η for *Bi*=50, k=10 and β=5. Curves show results based on the present model for the special case of constant *Bi*, while symbols show results from Yang & Vafai [11]. There is excellent agreement between the two. The present model is able to correctly predict the temperature bifurcation in the constant *Bi* case, as presented earlier by Yang & Vafai [11].

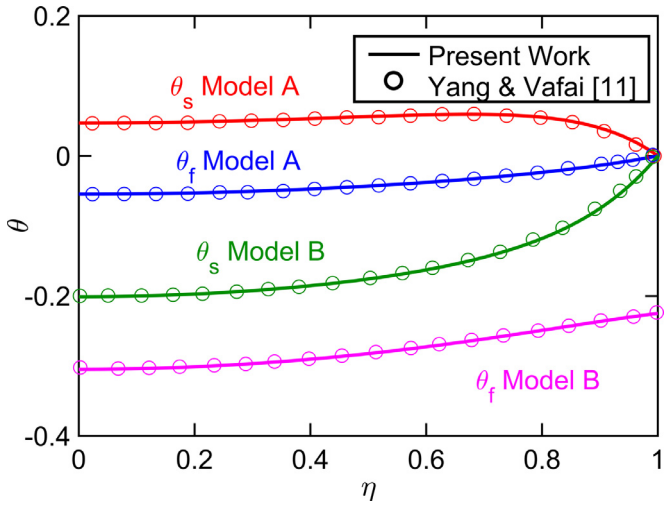

Fig. 2. Validation against past work by Yang & Vafai [11]: Temperature profiles, θ_f and θ_s, as a function of η for models A and B for the special case of constant *Bi*=50. Values of β and k are 5 and 10, respectively.

To further validate the present model, Nusselt number is calculated as a function of *Bi* and k for Model A. This is shown in Fig. 3(a) and (b) for two different values of the heat generation rate – β=5 and β=-0.5. These values are chosen to match the problem parameters used by Yang & Vafai [11]. Comparison of the present result with Yang & Vafai (please refer to Fig. 6(a) and (b) in their paper) shows that there is excellent agreement between the result presented here and the past work.

Figs. 2 and 3 demonstrate that the variable *Bi* model presented here agrees well with past work for the special case of constant *Bi*.

3.2. Temperature distribution for periodic and quadratic Bi

The model presented in Section 2 is used to plot solid and fluid temperature distributions for several different functions describing the variation of *Bi* within the channel. Specific functions of interest include sinusoidal and polynomial (quadratic) functions. Sinusoidal functions are of interest since any general well-behaved function can be represented by a series of sine functions with different frequencies.

Fig. 4 presents plots for solid and fluid temperatures in the channel for $Bi(\eta) = 50(1 + cos(2\pi\omega\eta))$, with k=1 and β=5. Results for Model A and Model B are presented in Fig. 4(a) and (b), respectively. Three different frequencies ω=1, 2 and 3 are considered. The periodic behavior of the temperature profile seen in both Fig. 4(a) and (b) is consistent with the periodicity of *Bi*. For example, for ω=1, both Fig. 4(a) and (b) shows maximum θ_s at η=0.55 and minimum θ_f at η=0.46, both close to the location of the minima for *Bi* at η=0.5. For ω=2, *Bi* has maxima at η=0.5, and two minima at η=0.25 and η=0.75. As expected, these lead to minimum and maximum temperature difference between the solid and fluid close to these locations, respectively, for both Models A and B as shown in Fig. 4(a) and (b). Results for ω=3 are similarly consistent. Note that in this case, the ratio of thermal conductivities of solid and fluid, k is 1, due to which, changes in θs and θ_f are of the same order. Also, note that the solid and fluid temperatures at the wall are both zero for Model A. On the other hand, only the solid temperature at the wall is zero for Model B, which is expected based on the wall boundary conditions.

Fig. 5 presents results for a similar problem with the same sinusoidal *Bi* as Fig. 4. However, in this case, k=10, which represents significant difference in thermal conductivity of the solid and fluid phases. Results for Models A and B are presented in Fig. 5(a) and (b), respectively. Similar to Fig. 4, these temperature profiles are consistent with the nature of *Bi* for different frequencies. Compared to Fig. 4, the much larger fluid phase thermal conductivity compared to that of the solid results in significant variation in θ_s but relatively smaller changes in θ_f. This is particularly evident for Model A, where the fluid temperature distribution is nearly the same over the entire η range for each of the three frequencies considered here. Similar to Fig. 4, solid and fluid temperatures converge to a value of zero at the wall for Model A. On the other hand, for Model B, only the solid temperature is zero at the wall.

Figs. 6 and 7 present similar analysis for a quadratically varying *Bi*, given by $Bi(\eta) = Bi_0(1 - \eta^2)$. The values of thermal conductivity ratio are k=1 and k=10 in Figs. 6 and 7, respectively. Results are presented for different values of Bi_0, and for both Models A and B. Both Figures show that the slope of the solid and fluid temperatures become zero at the centerline, which is expected from both mathematical equations and physical considerations for the problem. While *Bi* is modeled to be a function of space here, Fig. 6 shows that as the magnitude of Bi_0 increases, the difference between the solid and fluid temperatures reduces. This occurs be-

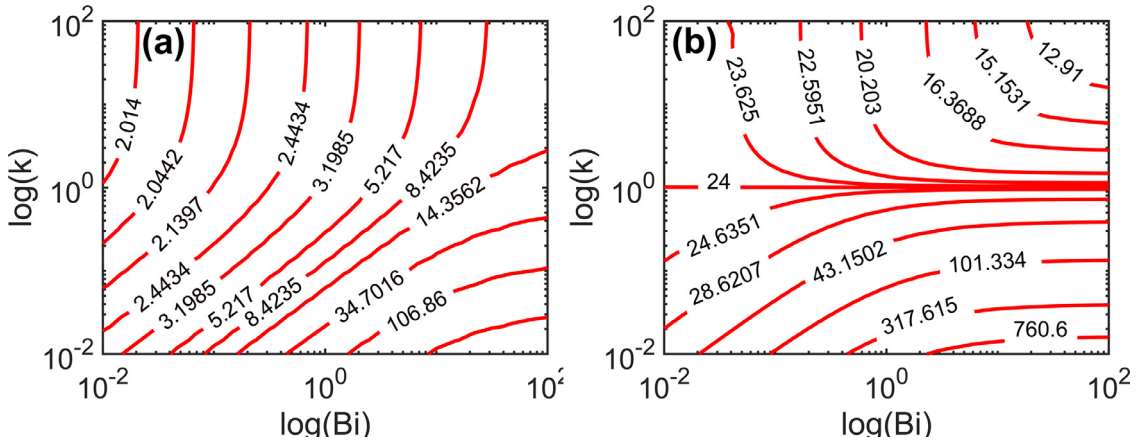

Fig. 3. Nusselt number as a function of k and Bi computed using the present work for the special case of constant Bi number: (a) β=5 and (b) β=-0.5.

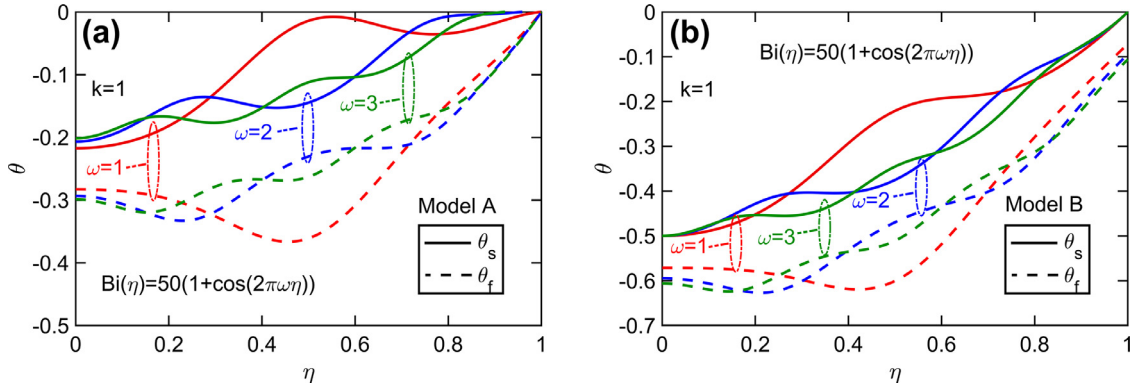

Fig. 4. Temperature distributions for periodic Bi: Plots of θ_f and θ_s as functions of η for $Bi(\eta) = 50(1 + cos(2\pi\omega\eta))$ with ω=1, 2 & 3, k=1, β=5. (a) Model A and (b) Model B.

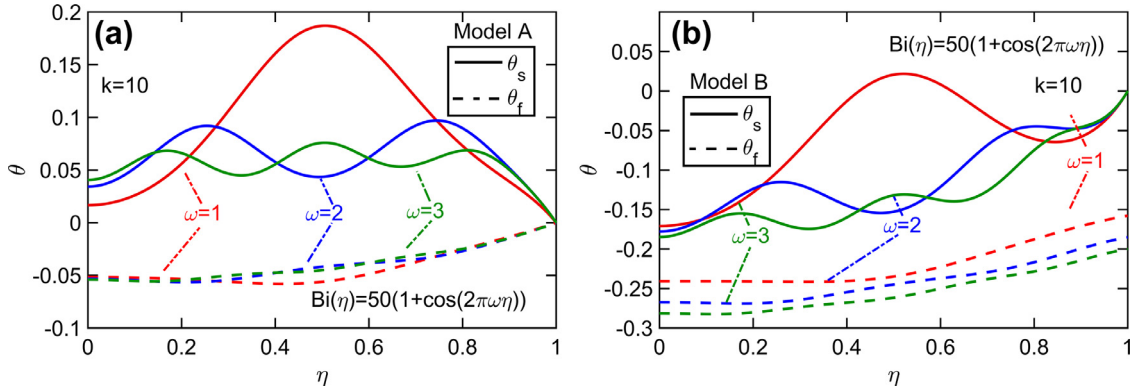

Fig. 5. Temperature distributions for periodic Bi: Plots of θ_f and θ_s as functions of η for $Bi(\eta) = 50(1 + cos(2\pi\omega\eta))$ with ω=1, 2 & 3, k=10, β=5. (a) Model A and (b) Model B.

cause a greater value of Bi_0 results in greater localized heat transfer between the two phases and thus greater thermal homogeneity. For Model A, the fluid and solid curves converge towards each other as η increases, and at the wall, the fluid and solid temperatures are equal to each other for model A. This is expected since model A explicitly requires fluid and solid temperatures to match at the wall. There is no such requirement for model B, which is why, the θ_f and θ_s curves in Figs. 6(b) and 7(b) do not converge at the wall.

It is instructive to compare Figs. 6(a) and 7(a) that present results for model A at two different values of k. This comparison shows that increasing the value of k results in weaker dependence of fluid temperature on the imposed Bi. This likely occurs due to larger fluid thermal conductivity compared to solid thermal conductivity at large value of k. On the other hand, the solid temperature becomes more strongly dependent on Bi as k increases. In comparison, Figs. 6(b) and 7(b) for model B show that the solid and fluid temperatures are not as strongly influenced by k in this case.

3.3. Nusselt number calculations

As discussed in Section 2.3, the value of Nusselt number is calculated for a number of scenarios involving sinusoidal and quadratic Bi variations. Fig. 8 plots Nu as a function of k for three different sinusoidal functions similar to ones considered in

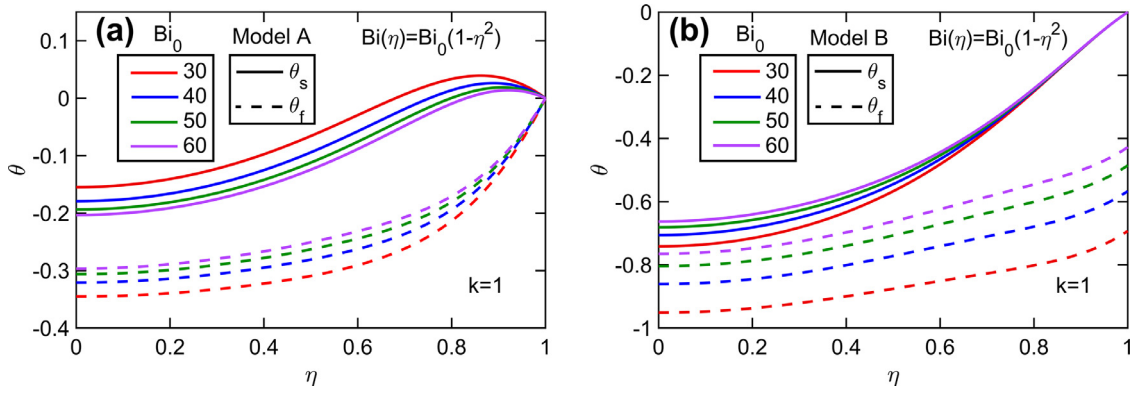

Fig. 6. Temperature distributions for parabolic *Bi*: Plots of θ_f and θ_s as functions of η for $Bi(\eta) = Bi_0(1-\eta^2)$ with different values *of* Bi_0 and k=1, β=5. (a) Model A and (b) Model B.

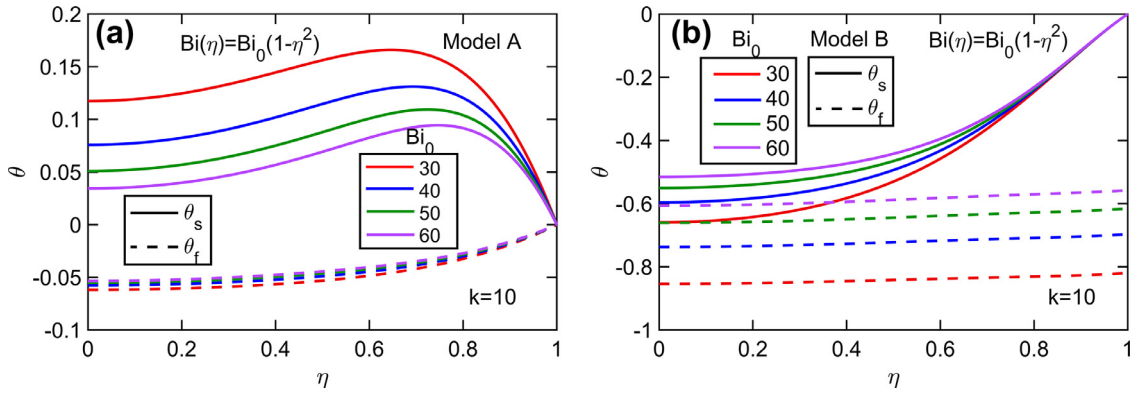

Fig. 7. Temperature distributions for parabolic *Bi*: Plots of θ_f and θ_s as functions of η for $Bi(\eta) = Bi_0(1-\eta^2)$ with different values *of* Bi_0 and k=10, β=5. (a) Model A and (b) Model B.

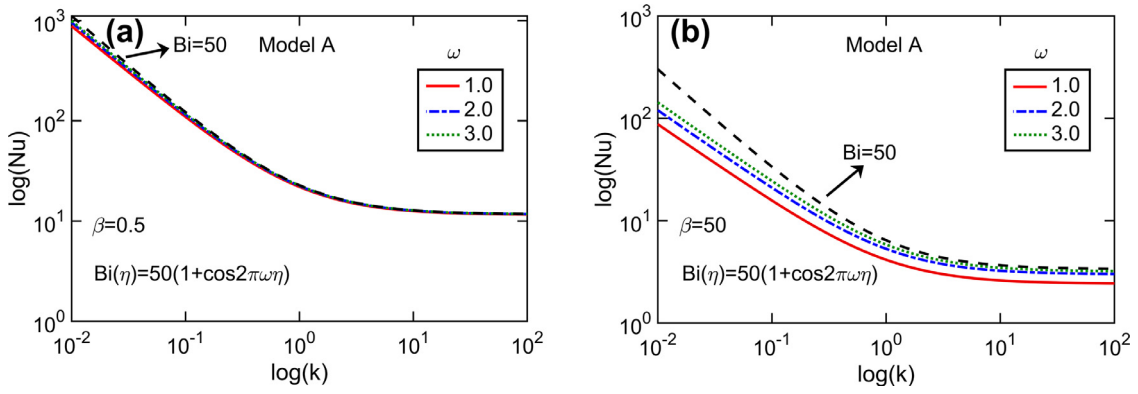

Fig. 8. Nusselt number as a function of k for $Bi(\eta) = 50(1 + cos(2\pi\omega\eta))$with ω=1,2 & 3: (a) β=0.5, (b) β=50. Both sub-plots are for Model A. The dashed line represents constant *Bi*=50 case for comparison.

Figs. 4 and 5. Fig. 8(a) and (b) plot these data for Model A and for β=0.5 and β=50, respectively. As expected, by using higher values for β that represents internal heat generation, the ability of the system to cool down the channel decreases. As a result, the Nusselt number decreases as β increases. Moreover, both figures show that by increasing the frequency, the overall Biot number becomes closer to the mean value of 50. As a result, the curves approach the constant *Bi* curve, also shown in Fig. 8(a) and (b), as frequency increases. An interesting observation is that by increasing the internal heat generation parameter β, the characteristic of the system goes more toward LTNE. Consequently, the curves shown in Fig. 8 are much more sensitive to the frequency of Biot number variation at the larger value of β considered here. On the other hand, at β =0.5, the frequency of *Bi* has lesser influence on *Nu*.

Fig. 9 examines the impact of internal heat generation parameter β on Nusselt number at two different values of thermal conductivity ratio k for model A. Both Fig. 9(a) and (b) show that increasing the internal heat generation rate decreases the overall cooling characteristic of the system, and consequently decreases *Nu*, which is as expected. The effect of frequency is also clearly seen in these Figures. Similar to Fig. 8, the curves approach the constant *Bi* curve as the frequency increases. It is interesting to note that in both figures, for low values of β, *Nu* is not strongly dependent on the frequency, whereas at larger values of β, the curves for three values of frequency are more distinct. Similar to

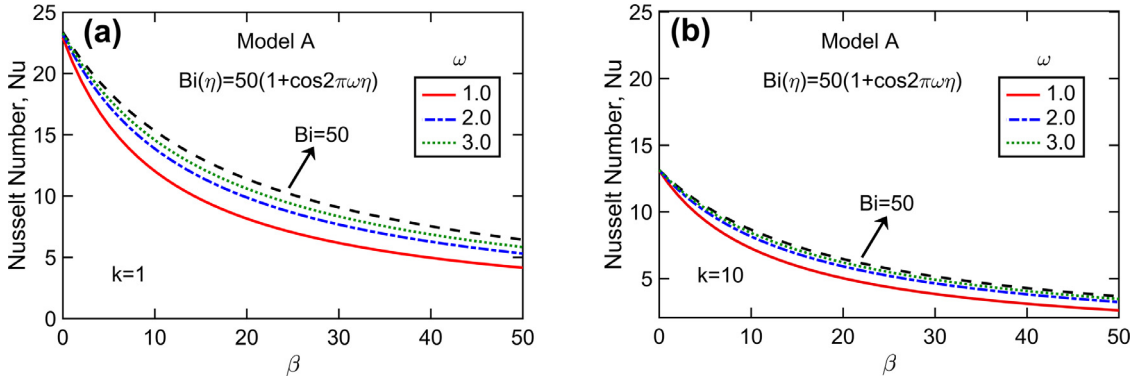

Fig. 9. Nusselt number as a function of β for $Bi(\eta) = 50(1 + cos(2\pi\omega\eta))$with ω=1,2 & 3: (a) k=1, (b) k=10. Both sub-plots are for Model A. The dashed line represents constant Bi=50 case for comparison.

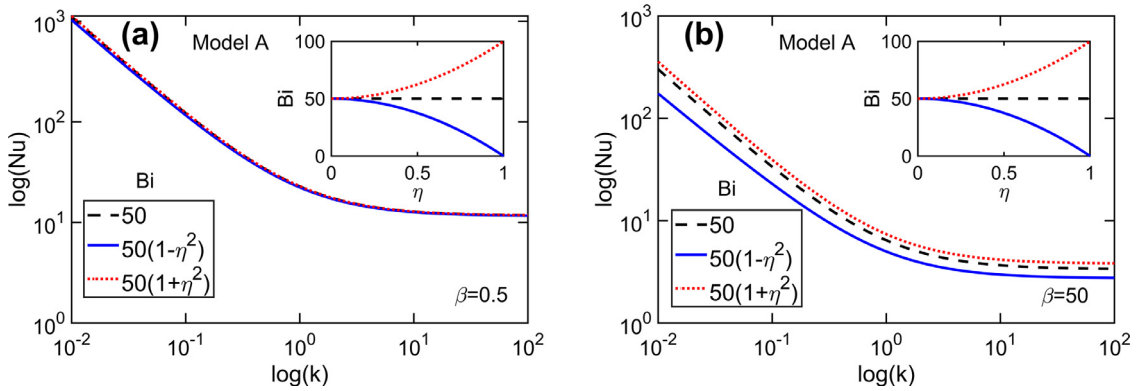

Fig. 10. Nusselt number as a function of k for $Bi(\eta) = 50$, $Bi(\eta) = 50(1 - \eta^2)$and $Bi(\eta) = 50(1 + \eta^2)$ for (a) β=0.5 and (b) β=50.

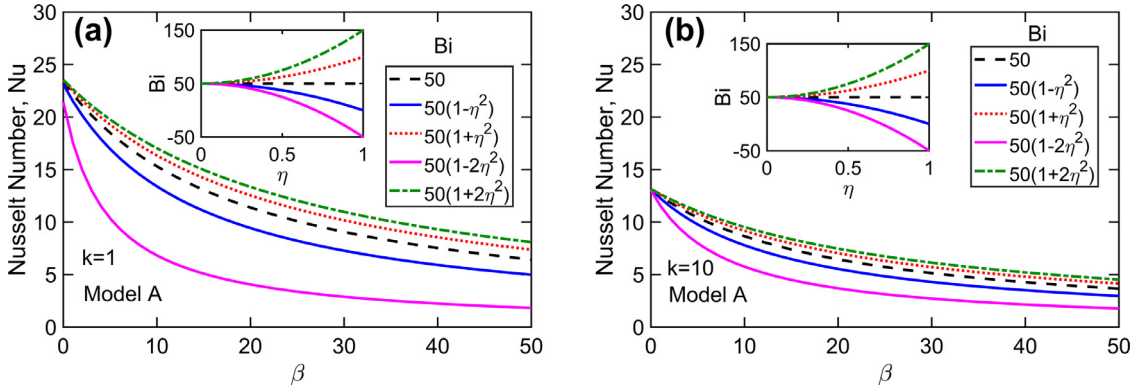

Fig. 11. Nusselt number as a function of β for $Bi(\eta) = 50$, $Bi(\eta) = 50(1 - \eta^2)$, $Bi(\eta) = 50(1 + \eta^2)$, $Bi(\eta) = 50(1 - 2\eta^2)$and $Bi(\eta) = 50(1 + 2\eta^2)$ for: (a) k=1 and (b) k=10.

Fig. 8, increasing the thermal conductivity ratio from 1 to 10, i.e., increasing the effective thermal conductivity of fluid compared to that of solid, results in reduction in *Nu*. This is particularly apparent for low internal heat generation values.

The dependence of *Nu* on various problem parameters for a quadratic *Bi* is presented in Figs. 10 and 11. Two specific functions $Bi=50(1-\eta^2)$ and $Bi=50(1+\eta^2)$ are considered and compared with the constant $Bi=50$ case. These functions increase and reduce the average value of *Bi* in the channel, respectively. Similar to Figs. 8 and 9, Fig. 10 examines the dependence of *Nu* on *k* for two different values of β, and Fig. 11 presents the dependence of *Nu* on β for two different values of *k*. These results show that the positive quadratic function $Bi=50(1+\eta^2)$ results in more homogeneous temperature within the porous medium, thereby resulting in increased value of *Nu*. On the other hand, temperature becomes less homogeneous, and therefore, *Nu* decreases when the negative quadratic function $Bi=50(1-\eta^2)$ is used. This effect is more pronounced for larger values of β. Fig. 11 presents similar plots for multiple functions $Bi=50(1\pm A\eta^2)$, with A=1 and 2. Similar to Figs. 8 and 9, the curves deviate more and more from the constant *Bi* case as the value of *A* increases.

4. Conclusions

Local thermal non-equilibrium (LTNE) is an important model for understanding and optimizing thermal and flow phenomena in a porous medium. With the advent of functionally graded materials, it is becoming possible to design porous materials with spatially distributed properties. This necessitates the development of LTNE models that account for such spatial distribution. The present work addresses this need by accounting for spatial variation in the Biot number, which, in past work, has always been assumed to be in-

variant. The resulting governing equations for the fluid and solid temperatures represent generalizations of past, constant *Bi* work, and account for arbitrary variations in *Bi* within the channel. The equations are solved for a variety of *Bi* functions. Specifically, for periodic *Bi*, the locations of maxima and minima in temperature fields are found to be well correlated with corresponding maxima and minima in the *Bi* function.

This work assumes that the functional gradient in the porous material causing the variation of Biot number does not impact the velocity distribution. This can be achieved by choosing functionally graded material or manufacturing the porous structure in such a way that porosity and permeability of the porous medium would provide the original velocity distribution. Also, if the thermal conductivity of the fluid and solid phases are similar, the LTNE model can be simplified to LTE model and hence much less complicated equations could be considered.

In addition to improving the theoretical understanding of thermal transport in porous materials, it is expected that the present work will help improve the thermal performance of novel porous materials with engineered properties.

Declaration of Competing Interest

None

CRediT authorship contribution statement

Mohammad Parhizi: Methodology, Formal analysis, Investigation, Data curation, Visualization, Writing - original draft, Writing - review & editing. **Mohsen Torabi:** Methodology, Data curation, Visualization, Writing - original draft, Writing - review & editing. **Ankur Jain:** Conceptualization, Methodology, Supervision, Project administration, Data curation, Visualization, Writing - original draft, Writing - review & editing.

Acknowledgment

This material is based upon work supported by CAREER Award No. CBET-1554183 from the National Science Foundation.

References

[1] M. Kaviany, 'Principles of Heat Transfer in Porous Media,' third ed., Springer, 2012.
[2] K. Vafai, third ed., CRC Press, 2015.
[3] P. Vadász (Ed.), 'Emerging Topics in Heat and Mass Transfer in Porous Media,', Spring, 2008.
[4] D. Ingham, I. Pop, Transport Phenomena in Porous Media (1998).
[5] G. Hetsroni, M. Gurevich, R. Rozenblit, Sintered porous medium heat sink for cooling of high-power mini-devices, Int. J. Heat and Fluid Flow 27 (2006) 259–266.
[6] A. Settari, Physics and modeling of thermal flow and soil mechanics in unconsolidated porous media, SPE Prod. Eng 7 (1992), doi:10.2118/18420-PA.
[7] H. Arkin, L. Xu, K. Holmes, Recent developments in modeling heat transfer in blood perfused tissues, IEEE Trans. Biomed. Eng. 41 (1994) 97–107.
[8] S. Pal, M. Hajj, W. Wong, I. Puri, Thermal energy storage in porous materials with adsorption and desorption of moisture, Int. J. Heat Mass Transf. 69 (2014) 285–292.
[9] M. Hunt, C. Tien, Non-Darcian convection in cylindrical packed beds, J. Heat Transf. 110 (1988) 378–384.
[10] A. Amiri, K. Vafai, Analysis of dispersion effects and non-thermal equilibrium non-Darcian, variable porosity incompressible flow through porous medium, Int. J. Heat Mass Transf. 37 (1994) 939–954.
[11] K. Yang, K. Vafai, Analysis of temperature gradient bifurcation in porous media – an exact solution, Int. J. Heat Mass Transf. 53 (2010) 4316–4325.
[12] H. Bortolozzi, J. Deiber, Comparison between two- and one-field models for natural convection in porous media, Chem. Eng. Sci. 56 (2001) 157–172.
[13] J. Wang, J. Shi, Discussion of boundary conditions of transpiration cooling problems using analytical solution of LTNE model., J. Heat Transf. 130 (2008) 1–5 014504.
[14] H. Xu, Z. Qu, T. Lu, Y. He, W. Tao, Thermal modeling of forced convection in a parallel-plate channel partially filled with metallic foams, J. Heat Transf. 133 (2011) 1–9 092603.
[15] H. Xu, Z. Qu, W. Tao, Analytical solution of forced convective heat transfer in tubes partially filled with metallic foam using the two-equation model, Int. J. Heat Mass Transf. 54 (2011) 3846–3855.
[16] Y. Mahmoudi, N. Karimi, Numerical investigation of heat transfer enhancement in a pipe partially filled with a porous material under local thermal nonequilibrium condition, Int J. Heat Mass Transf. 68 (2014) 161–173.
[17] Y. Mahmoudi, N. Karimi, K. Mazaheri, Analytical investigation of heat transfer enhancement in a channel partially filled with a porous material under local thermal non-equilibrium condition: effects of different thermal boundary conditions at the porous-fluid interface, Int. J Heat Mass Transf. 70 (2014) 875–891.
[18] M. Torabi, K. Zhang, G. Yang, J. Wang, P. Wu, Heat transfer and entropy generation analyses in a channel partially filled with porous media using local thermal non-equilibrium model, Energy 82 (2015) 922–938.
[19] M. Dehghan, M.S. Valipour, A. Keshmiri, S. Saedodin, N. Shokri, On the thermally developing forced convection through a porous material under the local thermal non-equilibrium condition: an analytical study, Int. J. Heat Mass Transf. 92 (2016) 815–823.
[20] M. Dehghan, M.S. Valipour, S. Saedodin, Y. Mahmoudi, Investigation of forced convection through entrance region of a porous-filled microchannel: an analytical study based on the scale analysis, Appl. Therm. Eng. 99 (2016) 446–454.
[21] M. Dehghan, M.S. Valipour, S. Saedodin, Analytical study of heat flux splitting in micro-channels filled with porous media, Transp. Porous Media 109 (2015) 571–587.
[22] M. Dehghan, M.S. Valipour, S. Saedodin, Conjugate heat transfer inside microchannels filled with porous media: an exact solution, J. Thermophys. Heat Transf. 30 (2016) 814–824.
[23] A. Fathi-kelestani, M. Nazari, Y. Mahmoudi, Pulsating flow in a channel filled with a porous medium under local thermal non-equilibrium condition: an exact solution, J. Therm. Anal. Calorim. (2020), doi:10.1007/s10973-020-09843-0.
[24] A. Amiri, K. Vafai, T.M. Kuzay, Effect of boundary conditions on non-Darcian heat transfer through porous media and experimental comparisons, Numer. Heat Transf. J. A 27 (1995) 651–664.
[25] B. Alazmi, K. Vafai, Constant wall heat flux boundary conditions in porous media under local thermal non-equilibrium conditions, Int. J. Heat Mass Transf. 45 (2002) 3071–3087.
[26] K. Yang, K. Vafai, Restrictions on the validity of the thermal conditions at the porous-fluid interface—an exact solution, J. Heat Transf. 133 (2011) 112601.
[27] D. Guthrie, M. Torabi, N. Karimi, Combined heat and mass transfer analyses in catalytic microreactors partially filled with porous material - the influences of nanofluid and different porous-fluid interface models, Int. J. Therm. Sci. 140 (2019) 96–113.
[28] I. Matula, G. Dercz, J. Barczyk, Titanium/Zirconium functionally graded materials with porosity gradients for potential biomedical applications, Mater. Sci. Technol. 36 (2020) 972–977.
[29] A.V. Kuznetsov, D.A. Nield, Local thermal non-equilibrium effects on the onset of convection in an internally heated layered porous medium with vertical throughflow, Int. J. Therm. Sci. 92 (2015) 97–105.
[30] Z.G. Xu, J. Qin, X. Zhou, H.J. Xu, Forced convective heat transfer of tubes sintered with partially-filled gradient metal foams (GMFs) considering local thermal non-equilibrium effect, Appl. Therm. Eng. 137 (2018) 101–111.
[31] D.A. Nield, A. Bejan, Convection in Porous Media, fourth ed., Springer, New York, 2013.
[32] C.T. Hsu, P. Cheng, Thermal dispersion in a porous medium, Int. J. Heat Mass Transf. 33 (1990) 1587–1597.